Nuclear Science and Engineering

ISSN: 0029-5639 (Print) 1943-748X (Online) Journal homepage: http://www.tandfonline.com/loi/unse20

An Accurate Globally Conservative Subdomain Discontinuous Least-Squares Scheme for Solving Neutron Transport Problems

Weixiong Zheng, Ryan G. McClarren & Jim E. Morel

To cite this article: Weixiong Zheng, Ryan G. McClarren & Jim E. Morel (2018) An Accurate Globally Conservative Subdomain Discontinuous Least-Squares Scheme for Solving Neutron Transport Problems, Nuclear Science and Engineering, 189:3, 259-271, DOI: 10.1080/00295639.2017.1407592

To link to this article: https://doi.org/10.1080/00295639.2017.1407592

Published online: 13 Dec 2017.

NUCLEAR SCIENCE AND ENGINEERING · VOLUME 189 · 259–271 · MARCH 2018

DOI: https://doi.org/10.1080/00295639.2017.1407592

An Accurate Globally Conservative Subdomain Discontinuous Least-Squares Scheme for Solving Neutron Transport Problems

Weixiong Zheng,*[a] Ryan G. McClarren,[b] and Jim E. Morel[b]

[a]*University of California, Berkeley, Nuclear Engineering, Berkeley, California 94709*
[b]*Texas A&M University, Nuclear Engineering, College Station, Texas 77843-3133*

Received December 6, 2016
Accepted for Publication November 16, 2017

Abstract — *In this work, we present a subdomain discontinuous least-squares (SDLS) scheme for neutronics problems. Least-squares (LS) methods are known to be inaccurate for problems with sharp total cross-section interfaces. In addition, the LS scheme is known not to be globally conservative in heterogeneous problems. In problems where global conservation is important, e.g., k-eigenvalue problems, a conservative treatment must be applied. In this study, we propose an SDLS method that retains global conservation and, as a result, gives high accuracy on eigenvalue problems. Such a method resembles the LS formulation in each subdomain without a material interface and differs from LS in that an additional LS interface term appears for each interface. The scalar flux is continuous in each subdomain with the continuous finite element method while discontinuous on interfaces for every pair of contiguous subdomains. The SDLS numerical results are compared with those obtained from other numerical methods with test problems having material interfaces. High accuracy of scalar flux in fixed-source problems and k_{eff} in eigenvalue problems is demonstrated.*

Keywords — *Global conservation, least squares, discrete ordinates.*

Note — *Some figures may be in color only in the electronic version.*

I. INTRODUCTION

Neutral particle transport problems are governed by a first-order, hyperbolic equation. As a result, particle transport problems, especially those that are streaming dominated, can have sharp gradients along the characteristic lines. Such problems require spatial discretizations that allow for discontinuities in space. Moreover, in regions where there is a strong scattering, the discontinuous finite element method (DFEM) has been shown to properly preserve the asymptotic diffusion limit of the transport equation.[1] These two facts have led to discontinuous Galerkin finite elements being widely accepted in transport calculations. Nevertheless, the DFEMs have more degrees of freedom (DoFs) than their continuous counterparts, especially in three dimensions.

Another approach to solving transport problems involves forming a second-order transport operator and solving the resulting equations using continuous finite elements. Second-order transport problems based on the parity of the equations and the self-adjoint angular flux (SAAF) equation are well know.[2–6] The resulting equations are symmetric but in void regions are ill posed and in near voids are ill conditioned.

More recently, Hansen et al.[7] derived a second-order form that is equivalent to minimizing the squared residual of the transport operator; it is therefore called the least-squares (LS) transport equation. This method can also be formed by multiplying the transport equation by the adjoint transport operator or by applying LS finite elements in space to the transport equation. The resulting equations in void are well posed and are symmetric positive definite (SPD). The LS method has been continuously investigated in the applied mathematics and computational

*E-mail: weixiong.zheng.uc.berkeley@gmail.com

fluid dynamics communities for decades.[8–13] However, the method generally has low accuracy in problems with interfaces between optically thin and thick materials without local refinement near the interfac.[14–17] Additionally, the standard LS method does not have particle conservation (except in the limit as the number of zones goes to infinity), which would induce undesirably large k-eigenvalue errors in neutronics simulations,[18] unless conservative acceleration schemes, such as nonlinear diffusion acceleration described in Refs. 19, 20, and 21, are applied to regain the conservation.

In the process of deriving the LS equations, the symmetrization of the transport equation converts a hyperbolic equation to an elliptic equation and causes loss of causality. For example, the presence of a strong absorber downstream of a source can influence the solution upstream of the source. In remedying this deficiency, it is desirable to add back some asymmetry to the operator but to do so in such a way that still preserves the positive properties of the LS method.

To this end, we develop a LS method that minimizes the square of the transport residual over certain regions of the entire problem domain. In each of these subregions, the interaction cross sections are slowly varying functions of space. We allow the solution between these regions to be discontinuous. The resulting scheme essentially solves LS independently in each subregion, and the regions are coupled through a sweeplike procedure.[a] Furthermore, with the correct weighting in the LS procedure, we can construct a method that is globally conservative.

The reminder of the paper is organized as follows. We start off reviewing the governing equation and the ordinary LS finite element weak formulation derived from the minimization point of view in Sec. II. In Sec. III, we propose a new method that is based on a LS formulation over contiguous blocks in the problem base on a novel subdomain-discontinuous functional. We also derive the corresponding weak formulations in this section. Next, we further theoretically demonstrate that the method, unlike standard LS methods, retains conservation in both a global sense and a subdomain sense. In Sec. IV, several numerical tests are presented to demonstrate conservation as well as the improved accuracy. We then conclude the study and discuss potential future work in Sec. V.

[a] In this work, we will utilize the discrete ordinates method for angular discretization. When solving the discrete ordinates equations with first-order discretization techniques, such as the discontinuous Galerkin method, the procedure is such that the transport equation is solved from upstream cells to downstream cells, which is a procedure called a "sweep."

II. REVISIT LS DISCRETIZATION OF TRANSPORT EQUATION

II.A. One-Group Transport Equation

We will consider steady, energy-independent transport problems with isotropic scattering in this work. The complications of energy dependence and anisotropic scattering can be readily incorporated into our method. The steady transport equation used to describe neutral particles of a single speed is expressed in operator form as

$$L\psi = q_s \ , \tag{1a}$$

where the transport operator L is defined as the sum of the streaming operator $\vec{\Omega}\cdot\nabla(\cdot)$ and total collision operator σ_t:

$$L = \vec{\Omega}\cdot\nabla(\cdot) + \sigma_t \ , \tag{1b}$$

and q_s represents the total volumetric source defined as the sum of the scattering source $S\psi$ and a fixed volumetric source $q(\vec{r},\vec{\Omega})$:

$$q_s = S\psi + q \, . \tag{1c}$$

In these equations $\psi(\vec{r},\vec{\Omega})$ is the angular flux of neutral particles with units of particles per unit area per unit time, where $\vec{r}\in\mathcal{D}\subset\mathbb{R}^3$, $\mathcal{D}$ stands for problem domain, and $\vec{\Omega}\in\mathbb{S}_2$ is a point on the unit sphere representing a direction of travel for the particles. S is the scattering operator. For isotropic scattering, it is defined as

$$S\psi = \int_{4\pi} d\Omega' \, \sigma_s\left(\vec{\Omega}\cdot\vec{\Omega}'\right)\psi(\vec{r},\vec{\Omega}') = \frac{\sigma_s\phi}{4\pi} \ , \tag{2}$$

where $\sigma_s\left(\vec{\Omega}\cdot\vec{\Omega}'\right)$ is the differential scattering cross section defined as

$$\sigma_s\left(\vec{\Omega}\cdot\vec{\Omega}'\right) = \frac{\sigma_s}{4\pi} \tag{3}$$

and ϕ is the scalar flux defined as

$$\phi = \int_{4\pi} d\Omega \, \psi \, . \tag{4}$$

Additionally, σ_s is the scattering cross section.

The boundary conditions for Eq. (1) specify the angular flux ψ^{inc} on the boundary for incoming directions:

$$\psi(\vec{r},\vec{\Omega}) = \psi^{inc}(\vec{r},\vec{\Omega}) \quad \text{for} \quad r \in \partial\mathcal{D}, \quad \vec{n}\cdot\vec{\Omega} < 0\,. \tag{5}$$

We discretize the angular component of the transport equation using the discrete ordinates S_N method.[22] Therein, we use a quadrature set $\{w_m, \vec{\Omega}_m\}$, containing weights w_m and quadrature collocation points $\vec{\Omega}_m$, for the angular space to obtain the set of equations:

$$\vec{\Omega}_m \cdot \nabla\psi_m + \sigma_t\psi_m = q_s, \quad \psi_m = \psi\left(\vec{\Omega}_m\right), \quad m = 1,\cdots,M\,, \tag{6}$$

with M being the total number of angles in the quadrature. Additionally, the angular integration for generic function f is defined as

$$\int_{4\pi} d\Omega f(\vec{\Omega}) = \sum_{m=1}^{M} w_m f(\vec{\Omega}_m)\,. \tag{7}$$

For instance, the scalar flux is expressed as

$$\phi(\vec{r}) = \int_{4\pi} d\Omega\,\psi(\vec{r},\vec{\Omega}) \approx \sum_{m=1}^{M} w_m\,\psi_m(\vec{r})\,. \tag{8}$$

II.B. Least-Squares Weak Formulation

In order to employ the continuous finite element method (CFEM) to solve the transport equation, Hansen et al.[7] derived a LS form of the transport equation by multiplying the transport equation by the adjoint streaming and removal operator, i.e.,

$$L^{\dagger}(L\psi - q_s) = 0\,, \tag{9}$$

where

$$L^{\dagger} = -\vec{\Omega}\cdot\nabla(\cdot) + \sigma_t\,. \tag{10}$$

The corresponding weak form of the problem in Eq. (9) with CFEM is the following: Given a function space $\mathcal{V}$, find $\psi \in \mathcal{V}$ such that $\forall v \in \mathcal{V}$:

$$\oint_{4\pi} d\Omega \int_{\mathcal{D}} dV v L^{\dagger}(L\psi - q_s) = 0\,. \tag{11}$$

The property of adjoint operators allows us to express Eq. (11) as

$$\oint_{4\pi} d\Omega \int_{\mathcal{D}} dV L v (L\psi - q_s) - \oint_{4\pi} d\Omega \int_{\partial\mathcal{D}} ds\,\vec{n}\cdot\vec{\Omega} v(L\psi - q_s) = 0\,. \tag{12}$$

Additionally, we require the transport equation to be satisfied on the boundary as well:

$$L\psi - q_s = 0\,. \tag{13}$$

Therefore, the weak form can be expressed as

$$\oint_{4\pi} d\Omega \int_{\mathcal{D}} dV L v (L\psi - q_s) = 0\,. \tag{14}$$

On the other hand, one could also derive the weak form from defining a LS functional of the transport residual:

$$\Gamma_{\text{LS}} = \frac{1}{2}\oint_{4\pi} d\Omega \int_{\mathcal{D}} dV (L\psi - q_s)^2\,. \tag{15}$$

Minimizing Eq. (15) in a discrete function space $\mathcal{V}$ leads to Eq. (14) as well.[b]

II.C. Imposing Boundary Conditions

In the derivation above, the incident boundary conditions have been ignored. Though it is possible to impose a strong boundary condition,[5] a weak boundary condition is chosen in this work instead. To weakly impose the boundary condition, the functional is changed to

$$\Gamma_{\text{LS}} = \frac{1}{2}\oint_{4\pi} d\Omega \int_{\mathcal{D}} dV (L\psi - q_s)^2 + \frac{1}{2}\int_{\vec{n}\cdot\vec{\Omega}<0} d\Omega \int_{\partial\mathcal{D}} ds\,\lambda\left(\psi - \psi^{inc}\right)^2\,, \tag{16}$$

where λ is a freely chosen Lagrange multiplier. The resulting LS weak formulation with the boundary condition is then expressed as

[b] The procedure of the minimization is to find a stationary "point" in a specific function space; see Ref. 23 for details.

$$\oint_{4\pi} d\Omega \int_{\mathcal{D}} dVLv(L-S)\psi + \int_{\vec{n}\cdot\vec{\Omega}<0} d\Omega \int_{\partial\mathcal{D}} ds\,\lambda v\psi = \oint_{4\pi} d\Omega \int_{\mathcal{D}} dVLvq + \int_{\vec{n}\cdot\vec{\Omega}<0} d\Omega \int_{\partial\mathcal{D}} ds\,\lambda v\psi^{inc}\,, \tag{17}$$

where the weight function v is any element of the trial space.

If we choose $\lambda = \sigma_t\left|\vec{n}\cdot\vec{\Omega}\right|$, then in nonvoid situations the LS scheme is globally conservative in homogeneous media (i.e., where σ_t is spatially independent in the whole domain). This can be seen by taking the weight function v to be 1 in Eq. (17) and performing the integration over angle to get

$$\sigma_t \mathbf{B} = 0\,, \tag{18a}$$

$$\mathbf{B} := \left(\int_{\partial\mathcal{D}} ds\, j^{out} - \int_{\vec{n}\cdot\vec{\Omega}<0} d\Omega \int_{\partial\mathcal{D}} ds\,\left|\vec{n}\cdot\vec{\Omega}\right|\psi^{inc} + \int_{\mathcal{D}} dV(\sigma_a\phi - Q) \right)\,, \tag{18b}$$

and

$$j^{out} := \int_{\vec{n}\cdot\vec{\Omega}>0} d\Omega\,\left|\vec{n}\cdot\vec{\Omega}\right|\psi \quad \text{and} \quad Q := \int_{4\pi} d\Omega\, q\,. \tag{18c}$$

Here, $\mathbf{B}$ is the global balance: It states that the outgoing current j^{out} plus the absorption $\sigma_a\phi$ is equal to the total source plus the incoming current. When $\sigma_t = 0$, $\mathbf{B}$ being any value does not disturb $\sigma_t\mathbf{B} = 0$. In general, what we observe is $\mathbf{B} \neq 0$. Therefore, conservation is lost.

III. A LS DISCRETIZATION ALLOWING DISCONTINUITY ON SUBDOMAIN INTERFACE

III.A. The SDLS Functional and Weak Formulation

Given that LS is conservative when the cross sections are constant and nonvoid, we propose to reformulate the problem to solve using LS in subdomains where cross sections are constant. On the boundary of these subdomains, we connect the angular fluxes using an interface condition that allows the fluxes to be discontinuous. The result is a discretization that can be solved using a procedure analogous to transport sweeps where the sweeps are over subdomains instead of mesh zones.

In the context of a minimization problem, we can define a functional in the following form:

$$\begin{aligned}\Gamma_{\text{SDLS}} = {} & \frac{1}{2}\sum_{\mathcal{D}_i} \oint_{4\pi} d\Omega \int_{\mathcal{D}_i} dV(L_i\psi_i - q_{si})^2 \\ & + \frac{1}{2}\sum_{\mathcal{D}_i\cap\partial\mathcal{D}\neq\emptyset} \int_{\vec{n}_i\cdot\vec{\Omega}<0} d\Omega \\ & \times \int_{\partial\mathcal{D}\cap\mathcal{D}_i} ds\sigma_{ti}\left|\vec{n}_i\cdot\vec{\Omega}\right|(\psi_i - \psi^{inc})^2 \\ & + \frac{1}{2}\sum_{\mathcal{D}_i}\sum_{\mathcal{F}_{i,j}} \int_{\vec{n}_i\cdot\vec{\Omega}<0} d\Omega \\ & \times \int_{\mathcal{F}_{i,j}} ds\sigma_{ti}\left|\vec{n}_i\cdot\vec{\Omega}\right|(\psi_i - \psi_j)^2\,,\end{aligned} \tag{19}$$

where $\mathcal{F}_{i,j}$ is the interface between $\mathcal{D}_i$ and any contiguous subdomain $\mathcal{D}_j$. Accordingly, the variational problem turns to the following: Find ψ_i in a polynomial space $\mathcal{V}$ such that $\forall v_i \in \mathcal{V}$:

$$\begin{aligned}& \sum_{\mathcal{D}_i}\left(\oint_{4\pi} d\Omega \int_{\mathcal{D}_i} dVL_iv_i(L_i - S_i)\psi_i \right. \\ & \quad \left. + \sum_{\mathcal{F}_{i,j}} \sigma_{ti} \int_{\vec{n}_i\cdot\vec{\Omega}<0} d\Omega \int_{\mathcal{F}_{i,j}} ds\,\left|\vec{n}_i\cdot\vec{\Omega}\right| v_i\left(\psi_i - \psi_j\right) \right) \\ & \quad + \sum_{\mathcal{D}_i\cap\partial\mathcal{D}\neq\emptyset} \int_{\vec{n}_i\cdot\vec{\Omega}<0} d\Omega \int_{\partial\mathcal{D}\cap\mathcal{D}_i} ds\sigma_{ti}\left|\vec{n}_i\cdot\vec{\Omega}\right| v_i\psi_i \\ & = \sum_{\mathcal{D}_i} \oint_{4\pi} d\Omega \int_{\mathcal{D}_i} dVL_iv_iq_i \\ & \quad + \sum_{\mathcal{D}_i\cap\partial\mathcal{D}\neq\emptyset} \int_{\vec{n}_i\cdot\vec{\Omega}<0} d\Omega \int_{\partial\mathcal{D}\cap\mathcal{D}_i} ds\sigma_{ti}\left|\vec{n}_i\cdot\vec{\Omega}\right| v_i\psi^{inc}\,.\end{aligned} \tag{20}$$

Compared with the ordinary LS method as illustrated in Eq. (17), the subdomain discontinuous least-squares (SDLS) method does not enforce the continuity on the subdomain interface. That presents the possibility of combining the LS method and transport sweeps. For a given direction $\vec{\Omega}$, Eq. (20) can be written as a block-lower triangular system if no reentering interface manifests. Therein, each block is LS applied to a subdomain. The inversion of this system requires solving a LS system for each subdomain, connected via boundary angular fluxes.

III.B. Subdomain-Wise and Global Conservation

A favorable SDLS property is that both subdomain conservation and global conservation are preserved. The demonstration is similar to the derivation in Sec. II.C. Taking $v_i = 1$, $L_i v_i$ simplifies to

$$L_i v_i = \sigma_{ti} \,. \tag{21}$$

Accordingly, the SDLS weak form in Eq. (20) is transformed into

$$\begin{aligned}
&\sum_{\mathcal{D}_i} \left(\oint_{4\pi} d\Omega \int_{\mathcal{D}_i} dV \sigma_{ti}(L_i - S_i)\psi_i \right. \\
&\quad \left. + \sum_{\mathcal{F}_{i,j}} \int_{\vec{n}_i\cdot\vec{\Omega}<0} d\Omega \int_{\mathcal{F}_{i,j}} ds \left|\vec{n}_i\cdot\vec{\Omega}\right| \sigma_{ti}\left(\psi_i - \psi_j\right) \right) \\
&\quad + \sum_{\mathcal{D}_i\cap\partial\mathcal{D}\neq\emptyset} \int_{\vec{n}_i\cdot\vec{\Omega}<0} d\Omega \int_{\partial\mathcal{D}\cap\mathcal{D}_i} ds \sigma_{ti} \left|\vec{n}_i\cdot\vec{\Omega}\right| \psi_i \\
&= \sum_{\mathcal{D}_i} \oint_{4\pi} d\Omega \int_{\mathcal{D}_i} dV \sigma_{ti} q_i \\
&\quad + \sum_{\mathcal{D}_i\cap\partial\mathcal{D}\neq\emptyset} \int_{\vec{n}_i\cdot\vec{\Omega}<0} d\Omega \int_{\partial\mathcal{D}\cap\mathcal{D}_i} ds \sigma_{ti} \left|\vec{n}_i\cdot\vec{\Omega}\right| \psi^{inc} \,.
\end{aligned} \tag{22}$$

Denoting the boundary of subdomain $\mathcal{D}_i$ by $\partial\mathcal{D}_i$,[c] one may express the first integral in Eq. (22) as

$$\begin{aligned}
&\sum_{\mathcal{D}_i} \oint_{4\pi} d\Omega \int_{\mathcal{D}_i} dV \sigma_{ti}(L_i - S_i)\psi_i \\
&= -\sum_{\mathcal{D}_i} \int_{\partial\mathcal{D}_i} ds \int_{\vec{n}_i\cdot\vec{\Omega}<0} d\Omega \left|\vec{n}_i\cdot\vec{\Omega}\right| \sigma_{ti}\psi_i \\
&\quad + \sum_{\mathcal{D}_i} \int_{\partial\mathcal{D}_i} ds \int_{\vec{n}_i\cdot\vec{\Omega}>0} d\Omega \left|\vec{n}_i\cdot\vec{\Omega}\right| \sigma_{ti}\psi_i \\
&\quad + \sum_{\mathcal{D}_i} \int_{\mathcal{D}_i} dV \sigma_{ti}\sigma_{ai}\phi_i \,.
\end{aligned} \tag{23}$$

Note that

$$\begin{aligned}
&\sum_{\mathcal{D}_i} \sum_{\mathcal{F}_{i,j}} \int_{\vec{n}_i\cdot\vec{\Omega}<0} d\Omega \int_{\mathcal{F}_{i,j}} ds \left|\vec{n}_i\cdot\vec{\Omega}\right| \sigma_{ti}\psi_i \\
&\quad + \sum_{\mathcal{D}_i\cap\partial\mathcal{D}\neq\emptyset} \int_{\vec{n}_i\cdot\vec{\Omega}<0} d\Omega \int_{\partial\mathcal{D}\cap\mathcal{D}_i} ds \sigma_{ti} \left|\vec{n}_i\cdot\vec{\Omega}\right| \psi_i \\
&\quad - \sum_{\mathcal{D}_i} \int_{\partial\mathcal{D}_i} ds \int_{\vec{n}_i\cdot\vec{\Omega}<0} d\Omega \left|\vec{n}_i\cdot\vec{\Omega}\right| \sigma_{ti}\psi_i = 0 \,.
\end{aligned} \tag{24}$$

Introducing Eqs. (23) and (24) into Eq. (22) leads to

$$\begin{aligned}
&\sum_{\mathcal{D}_i} \left(\int_{\mathcal{D}_i} dV \, \sigma_{ti}\sigma_{ai}\phi_i + \sum_{\partial\mathcal{D}_i} \int_{\vec{n}_i\cdot\vec{\Omega}>0} d\Omega \int_{\mathcal{F}_{i,j}} ds \sigma_{ti} \left|\vec{n}_i\cdot\vec{\Omega}\right| \psi_i \right) \\
&= \sum_{\mathcal{D}_i} \sum_{\mathcal{F}_{i,j}} \int_{\vec{n}_i\cdot\vec{\Omega}<0} d\Omega \int_{\mathcal{F}_{i,j}} ds \left|\vec{n}_i\cdot\vec{\Omega}\right| \sigma_{ti}\psi_j + \sum_{\mathcal{D}_i} \int_{\mathcal{D}_i} dV \sigma_{ti} Q_i \\
&\quad + \sum_{\mathcal{D}_i\cap\partial\mathcal{D}\neq\emptyset} \int_{\vec{n}_i\cdot\vec{\Omega}<0} d\Omega \oint_{\partial\mathcal{D}\cap\mathcal{D}_i} ds \sigma_{ti} \left|\vec{n}_i\cdot\vec{\Omega}\right| \psi^{inc} \,.
\end{aligned} \tag{25}$$

Define the incoming currents from the contiguous subdomain $\mathcal{D}_j$, problem boundary for subdomain $\mathcal{D}_i$, and outgoing current as, respectively,

$$j^{in}_{i,j}(\vec{r}) := \int_{\vec{n}_i\cdot\vec{\Omega}<0} d\Omega \left|\vec{n}_i\cdot\vec{\Omega}\right| \psi_i \,, \tag{26a}$$

$$j^{in}_{i,b}(\vec{r}) := \int_{\vec{n}_i\cdot\vec{\Omega}<0} d\Omega \left|\vec{n}_i\cdot\vec{\Omega}\right| \psi^{inc} \,, \tag{26b}$$

and

$$j^{out}_{i}(\vec{r}) := \int_{\vec{n}_i\cdot\vec{\Omega}>0} d\Omega \left|\vec{n}_i\cdot\vec{\Omega}\right| \psi_i \,. \tag{26c}$$

Then, getting Eq. (27) is straightforward:

$$\begin{aligned}
&\sum_{\mathcal{D}_i} \left(\int_{\mathcal{D}_i} dV \sigma_{ti}\sigma_{ai}\phi_i + \int_{\partial\mathcal{D}_i} ds \sigma_{ti} j^{out}_i \right) \\
&= \sum_{\mathcal{D}_i} \sum_{\mathcal{F}_{i,j}} \int_{\mathcal{F}_{i,j}} ds \sigma_{ti} j^{in}_{i,j} + \sum_{\mathcal{D}_i\cap\partial\mathcal{D}\neq\emptyset} \int_{\partial\mathcal{D}\cap\mathcal{D}_i} ds \sigma_{ti} j^{in}_{i,b} \\
&\quad + \sum_{\mathcal{D}_i} \int_{\mathcal{D}_i} dV \sigma_{ti} Q_i \,.
\end{aligned} \tag{27}$$

[c] Note that $\partial\mathcal{D}_i$ could be on either the problem boundary or the interior interfaces.

Assuming σ_{ti} is spatially uniform within $\mathcal{D}_i$, we can further transform Eq. (27) to

$$\sum_{\mathcal{D}_i}\sigma_{ti}\left(\int_{\mathcal{D}_i}dV\sigma_{ai}\phi_i+\int_{\partial\mathcal{D}_i}ds j_i^{out}\right)-\sum_{\mathcal{D}_i}\sigma_{ti}\sum_{\mathcal{F}_{i,j}}\int_{\mathcal{F}_{i,j}}ds j_{i,j}^{in}-\sum_{\mathcal{D}_i\cap\partial\mathcal{D}\neq\emptyset}\sigma_{ti}\int_{\partial\mathcal{D}\cap\mathcal{D}_i}ds j_{i,b}^{in}-\sum_{\mathcal{D}_i}\sigma_{ti}\int_{\mathcal{D}_i}dVQ_i=0\,, \tag{28}$$

or equivalently,

$$\sum_{\mathcal{D}_i}\sigma_{ti}\mathbf{B}_i=0\,. \tag{29}$$

For all nonzero σ_{ti}, in order to make Eq. (29) true, one must have subdomain-wise conservation:

$$\mathbf{B}_i\equiv 0,\quad \forall\mathcal{D}_i\subset\mathcal{D}\,. \tag{30}$$

Additionally, this implies that there is the global conservation:

$$\sum_{\mathcal{D}_i}\mathbf{B}_i=0\,. \tag{31}$$

III.C. Conservative Void Treatment

CFEM-SAAF is globally conservative yet is not compatible with void and in near-void situations is potentially ill conditioned. Therefore, efforts have been put in alleviating CFEM-SAAF in void.[17,18,21,24] We will specially give a brief review of the treatment developed in Refs. 18 and 24.

Therein, Laboure et al. developed a hybrid method compatible with void and near void based on SAAF and LS. Denote nonvoid and void/uniform near-void subdomains by $\mathcal{D}_n$ and $\mathcal{D}_v$, respectively.[d] Then, the hybrid formulation is presented as

$$\begin{aligned}&\oint_{4\pi}d\Omega\int_{\mathcal{D}}dV\left(\tau\vec{\Omega}\cdot\nabla v\psi+\sigma_t v\psi-(1-\sigma_t\tau)\vec{\Omega}\cdot\nabla v\psi\right)+\int_{\vec{n}\cdot\vec{\Omega}>0}d\Omega\int_{\partial\mathcal{D}}ds\left|\vec{n}\cdot\vec{\Omega}\right|v\psi\\&\quad=\oint_{4\pi}d\Omega\int_{\mathcal{D}}dV\left(\tau\vec{\Omega}\cdot\nabla v+v\right)q_s+\int_{\vec{n}\cdot\vec{\Omega}<0}d\Omega\int_{\partial\mathcal{D}}ds\left|\vec{n}\cdot\vec{\Omega}\right|v\psi^{inc}\,,\end{aligned} \tag{32}$$

where

$$\tau=\begin{cases}1/\sigma_t, & \vec{r}\in\mathcal{D}_n\\ 1/c & \vec{r}\in\mathcal{D}_v\end{cases} \tag{33}$$

and c is a freely chosen constant and usually set to be 1. One notices that in the nonvoid subdomain, the formulation resembles CFEM-SAAF. At the same time, global conservation is preserved. Therefore, the method is named SAAF–conservative LS (CLS) (SAAF-CLS).

Consider a homogeneous near-void problem. The weak form in Eq. (32) can be transformed into

$$\begin{aligned}&\oint_{4\pi}d\Omega\int_{\mathcal{D}_v}dVLv(L\psi-q_s)+\int_{\vec{n}\cdot\vec{\Omega}<0}d\Omega\int_{\partial\mathcal{D}_v}ds\sigma_t\left|\vec{n}\cdot\vec{\Omega}\right|v(\psi-\psi^{inc})+\oint_{4\pi}d\Omega\int_{\mathcal{D}_v}dVcv(L\psi-q_s)\\&\quad+\int_{\vec{n}\cdot\vec{\Omega}<0}d\Omega\int_{\partial\mathcal{D}_v}dsc\left|\vec{n}\cdot\vec{\Omega}\right|v(\psi-\psi^{inc})=0\,.\end{aligned} \tag{34}$$

[d] In our work, $\mathcal{D}_v$ is defined with $\sigma_t<0.01\ \mathrm{cm}^{-1}$.

In void/near void, CLS is conservative:

$$(\sigma_t + c)\mathbf{B} = 0\,. \tag{35}$$

We therefore modify SDLS such that void treatment based on Eq. (34) is incorporated:

$$\begin{aligned}
&\sum_{\mathcal{D}_i\subset\mathcal{D}_n}\left(\oint_{4\pi} d\Omega \int_{\mathcal{D}_i} dV L_i v_i (L_i - S_i)\psi_i + \sum_{\mathcal{F}_{ij}} \sigma_{ti} \int_{\vec{n}_i\cdot\vec{\Omega}<0} d\Omega \int_{\mathcal{F}_{ij}} ds \left|\vec{n}_i\cdot\vec{\Omega}\right| v_i\left(\psi_i - \psi_j\right)\right)\\
&+ \sum_{\substack{\mathcal{D}_i\cap\partial\mathcal{D}\neq\emptyset\\ \mathcal{D}_i\subset\mathcal{D}_n}} \int_{\vec{n}_i\cdot\vec{\Omega}<0} d\Omega \int_{\partial\mathcal{D}\cap\mathcal{D}_i} ds\sigma_{ti}\left|\vec{n}_i\cdot\vec{\Omega}\right| v_i\psi_i\\
&+ \sum_{\mathcal{D}_i\subset\mathcal{D}_v}\left(\oint_{4\pi} d\Omega \int_{\mathcal{D}_i} dV (cv_i + L_i v_i)(L_i - S_i)\psi_i + \sum_{\mathcal{F}_{ij}} \int_{\vec{n}_i\cdot\vec{\Omega}<0} d\Omega \int_{\mathcal{F}_{ij}} ds(c+\sigma_{ti})\left|\vec{n}_i\cdot\vec{\Omega}\right| v_i\left(\psi_i - \psi_j\right)\right)\\
&+ \sum_{\substack{\mathcal{D}_i\cap\partial\mathcal{D}\neq\emptyset\\ \mathcal{D}_i\subset\mathcal{D}_v}} \int_{\vec{n}_i\cdot\vec{\Omega}<0} d\Omega \int_{\partial\mathcal{D}\cap\mathcal{D}_i} ds(c+\sigma_{ti})\left|\vec{n}_i\cdot\vec{\Omega}\right| v_i\psi_i\\
&= \sum_{\mathcal{D}_i\subset\mathcal{D}_n}\oint_{4\pi} d\Omega \int_{\mathcal{D}_i} dV L_i v_i q_i + \sum_{\substack{\mathcal{D}_i\cap\partial\mathcal{D}\neq\emptyset\\ \mathcal{D}_i\subset\mathcal{D}_n}} \int_{\vec{n}_i\cdot\vec{\Omega}<0} d\Omega \int_{\partial\mathcal{D}\cap\mathcal{D}_i} ds\sigma_{ti}\left|\vec{n}_i\cdot\vec{\Omega}\right| v_i\psi^{inc}\\
&+ \sum_{\mathcal{D}_i\subset\mathcal{D}_v}\oint_{4\pi} d\Omega \int_{\mathcal{D}_i} dV (cv_i + L_i v_i) q_i + \sum_{\substack{\mathcal{D}_i\cap\partial\mathcal{D}\neq\emptyset\\ \mathcal{D}_i\subset\mathcal{D}_v}} \int_{\vec{n}_i\cdot\vec{\Omega}<0} d\Omega \int_{\partial\mathcal{D}\cap\mathcal{D}_i} ds(c+\sigma_{ti})\left|\vec{n}_i\cdot\vec{\Omega}\right| v_i\psi^{inc}\,.
\end{aligned} \tag{36}$$

IV. NUMERICAL RESULTS

The implementation is carried out by the `deal.ii` C++ finite element library.[25] The bi-conjugate gradient stabilized method[26] is used as the linear solver for SDLS and CFEM-SAAF-CLS while LS and CFEM-SAAF are solved using the conjugate gradient method. Symmetric successive overrelaxation[27] is used as a preconditioner for all calculations with the relaxation factor fixed at 1.4. In all tests, we also include results from solving the globally conservative SAAF equation with CFEM as a comparison.[2,21] In all problems, piecewise linear polynomial basis functions are used. In the one-dimensional (1-D) examples, the angular quadrature is the Gauss quadrature. In the two-dimensional test, the quadrature is a Gauss-Chebyshev quadrature with an azimuthal point number on each polar level specified in a way similar to level-symmetric quadrature. See Ref. 28 for further details.

IV.A. Reed's Problem

The first problem is Reed's problem in 1-D slab geometry[29] designed to test spatial differencing accuracy and stability. The material properties are listed in Table I. Specifically, a void region is set at $x \in (3,\ 5)$. Results using S_8 in angle are presented in Fig. 1a with zoomed results for $x \in (4.75, 6.25)$ cm in Fig. 1b. In Fig. 1, 32 cells are used for the CFEM-LS (green dot-dash line), CFEM-SAAF-CLS (blue circle line), and SDLS (red triangle line) calculations. For SDLS, the interfaces

TABLE I

Material Configuration for Reed's Problem

x (cm)	(0, 2)	(2, 3)	(3, 5)	(5, 6)	(6, 8)
σ_t (cm^{-1})	1	1	0	5	50
σ_s (cm^{-1})	0.9	0.9	0	0	0
Q	0	1	0	0	5

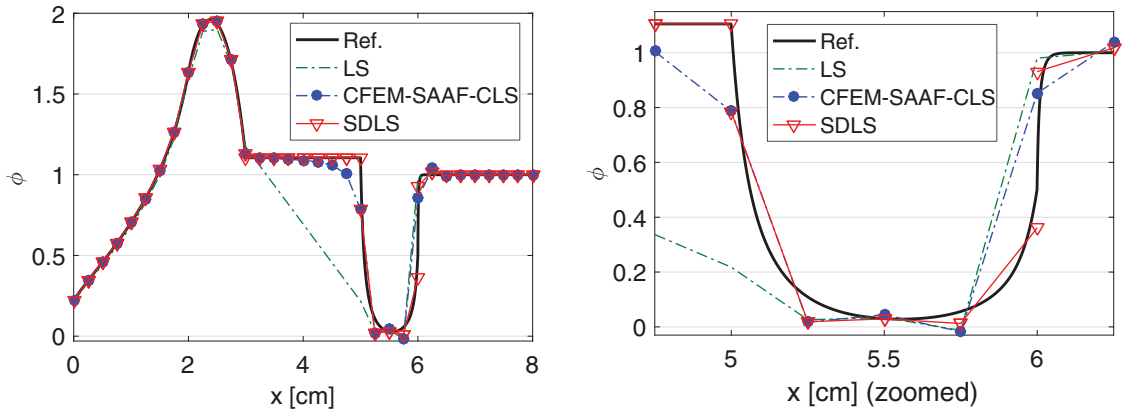

(a) Reed's problem result comparison.

(b) Zoomed results $x \in (4.75, 6.25)$ cm.

Fig. 1. Reed's problem results from different methods; 32 cells are used.

are set at $x = 3, 5, 6$ cm. The reference is provided by solving the first-order transport equation with DFEM with linear discontinuous basis using 2000 cells.

With the void treatment, the SDLS flux profile in $x \in (3, 5)$ is flat, and the relative error is lower than 3×10^{-5}. By defining the relative balance as

$$\mathbf{B}_{rel} = \frac{|\mathbf{B}|}{\int\limits_{\vec{n}\cdot\vec{\Omega}<0} d\Omega \int\limits_{\partial\mathcal{D}} ds \left|\vec{n}\cdot\vec{\Omega}\right|\psi^{inc} + \int\limits_{\mathcal{D}} dVQ} ,$$

we found that SDLS is globally conservative as $\mathbf{B}_{rel} = 5.56 \times 10^{-12}$. On the other hand, the LS solution is distorted in void, and the balance is poor ($\mathbf{B}_{rel} = 3.73 \times 10^{-3}$). Meanwhile, we notice that CFEM-SAAF-CLS gives a better solution in the graph norm than LS in most regions of the problem. Yet, the solution in the void region is heavily affected by the thick absorber [$x \in (5, 6)$ cm] as continuity is enforced at $x = 5$ cm.

IV.B. Two-Region Absorption Problem

Another test problem is a 1-D slab pure absorber problem first proposed by Zheng et al.[30] There is a unit isotropic incident angular flux on the left boundary of the slab. No source appears in the domain. In this problem,

$$\sigma_t = \begin{cases} 0.1\,\text{cm}^{-1} & x < 1\,\text{cm} \\ 10\ \text{cm}^{-1} & \text{otherwise} \end{cases} .$$

The results in Fig. 2 compare coarse solutions using different methods. The reference solution was computed with

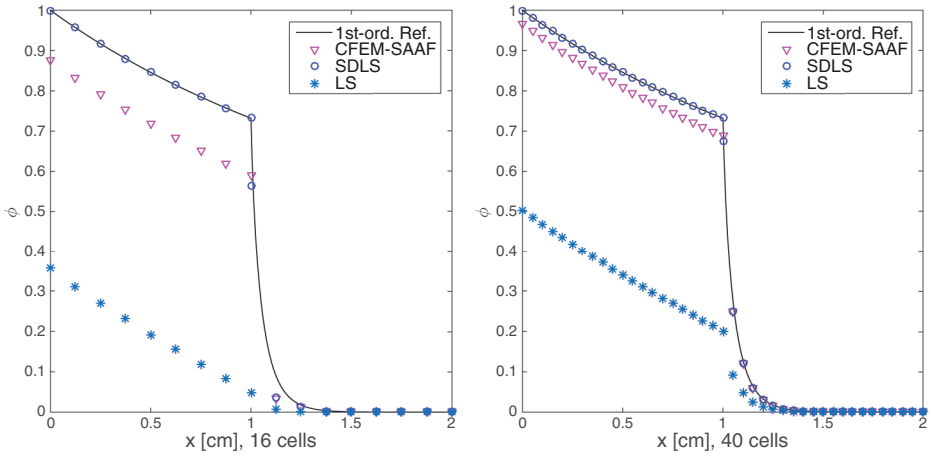

(a) 16 cells.

(b) 40 cells.

Fig. 2. Two-region absorption results comparison with LS, SAAF, and SDLS.

first-order S_8 using diamond difference using 2×10^4 spatial cells. The LS and SAAF solutions in the thin region ($x < 1$ cm) are affected by the presence of the thick region ($x > 1$ cm), even though that region is downstream of the incoming boundary source. Increasing the cell count does improve these solutions, but there is still significant discrepancy with the reference solution. In both cases, the SDLS solution captures the behavior of the reference solution. In Fig. 3 we see that LS, SDLS, and SAAF converge to the exact solution at second order, with the convergence for LS being a bit more erratic.

Table II presents the relative global balances for different methods. As expected, LS presents large balance errors, even when the mesh is refined. On the other hand, CFEM-SAAF and SDLS give round-off balance to the iterative solver tolerance as expected.

IV.C. Thin-Thick *k*-Eigenvalue Problem

A one-group k-eigenvalue problem is also tested in 1-D slab geometry. An absorber region in $x \in (0, 0.3)$ cm is set adjacent to a multiplying region in $x \in (0.3, 1.5)$ cm. Material properties are presented in Table III. Reflective boundary conditions are imposed on both sides of the slab. The configuration is to mimic the impact from setting a control rod near the fuel.

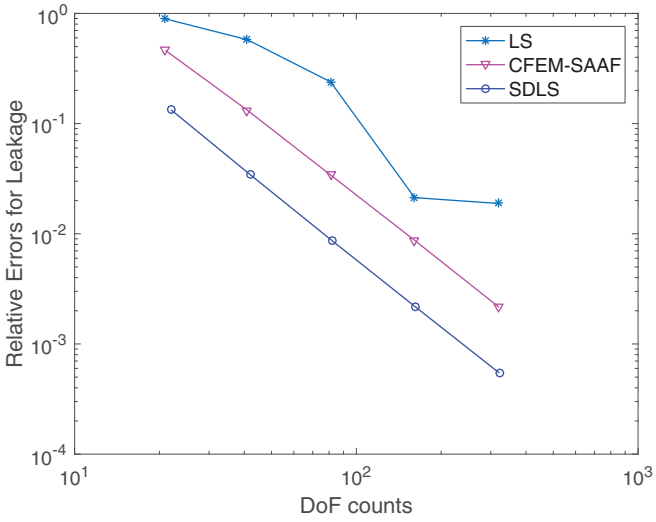

Fig. 3. Leakage errors versus DoF counts per direction at the right boundary.

A reference is provided by CFEM-SAAF using 20 480 spatial cells. With the presence of the strong absorber, the scalar flux has a large gradient near $x = 0.3$ cm. Figure 4 compares the results from the different methods using 20 spatial cells. In this case, LS (green starred line) presents noticeable undershooting near the subdomain interface. Though CFEM-SAAF (blue triangles) is an improvement, it is still away from the reference in the fuel region. SDLS (red squares), in contrast, agrees well with the reference solution except at the discontinuity introduced on the material interface set at $x = 0.3$ cm.

We also examine the k_{eff} in Fig. 5. We observe that SDLS converges to the reference k_{eff} in the graph norm using only ten spatial cells in Fig. 5a. Yet, CFEM-SAAF slowly converges to the reference, and LS still has a large error with 160 cells. Figure 5b shows k_{eff} error change with respect to DoF counts and illustrates the benefit of adding the subdomain interface discontinuity. With five cells (the points with the smallest DoF counts), SDLS has more than an order lower of k_{eff} error than CFEM-SAAF. When refining the spatial mesh, SDLS shows roughly second-order convergence and has an error three orders of magnitude lower than CFEM-SAAF with 160 cells (the points with the largest DoF counts) although both have the global conservations.

IV.D. One-Group Iron-Water Problem

The last test is a modified one-group iron-water shielding problem[31] used to test the accuracy of the numerical schemes in relatively thick materials (see the configuration in Fig. 6a). The material properties listed in Table IV are from the thermal group data. For the angular discretization, S_4 is used. The reference is SDLS using 1200×1200 cells (see the scalar flux in Fig. 6b). The scalar flux in the domain is rather smooth due to the scatterings. As a result, with

TABLE II

Relative Global Balances with Different Methods*

Number of Cells	20	40	80	160	320
LS	8.439×10^{-1}	6.426×10^{-1}	3.564×10^{-1}	3.430×10^{-1}	4.948×10^{-2}
CFEM-SAAF	5.899×10^{-14}	1.786×10^{-13}	2.615×10^{-13}	1.274×10^{-12}	5.599×10^{-12}
SDLS	2.148×10^{-13}	7.668×10^{-13}	1.492×10^{-12}	2.090×10^{-11}	2.704×10^{-12}

*In absolute values.

TABLE III

Material configuration for k-Eigenvalue Problem

x (cm)	(0, 0.5)	(0.5, 1.5)
σ_t (cm^{-1})	5	1
σ_s (cm^{-1})	0	0.99
$\nu\sigma_f$	0	0.25

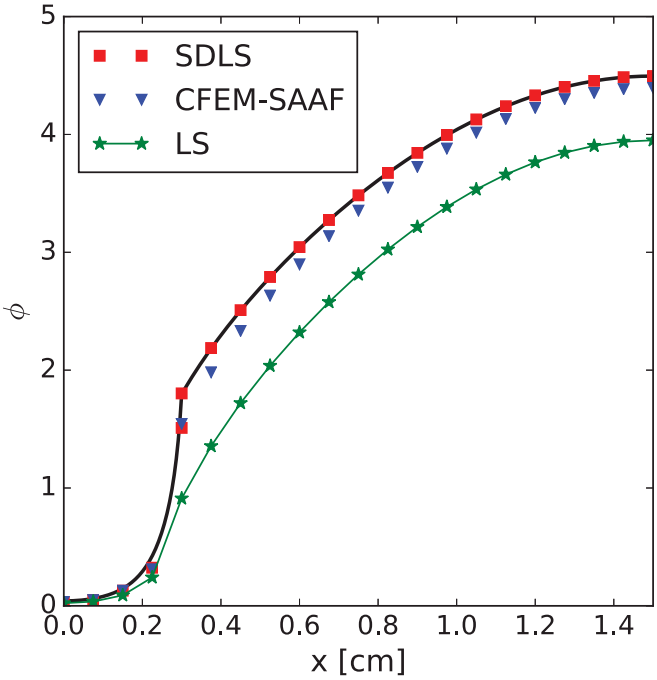

Fig. 4. Scalar flux from different methods.

moderately fine mesh (120 × 120 cells), we see that SDLS graphically agrees with CFEM-SAAF and LS in the line-out illustrated in Fig. 7a. We further examine the absorption rate errors in iron. As shown in Fig. 7b, LS and CFEM-SAAF present similar spatial convergence rates. However, LS presents lower accuracy than CFEM-SAAF with the presence of the material interface between iron and water. On the other hand, by setting two interfaces between iron and water and introducing extra DoFs on the subdomain interfaces, SDLS converges to the reference solution much earlier than the other methods.

In addition, we present a timing comparison of the different methods in Fig. 8 using the same error data employed in Fig. 7b. Both CFEM-SAAF and SDLS are more accurate given a specific computing time. For a specific high error level ($>3 \times 10^{-3}$) obtained using coarse meshes, SDLS is more time-consuming than CFEM-SAAF. However, for low error levels ($<3 \times 10^{-3}$) achieved by refining the mesh, SDLS cost much less total computing time than CFEM-SAAF. On the other hand, when the total computing time increases, the SDLS error drops faster than both CFEM-SAAF and LS. Overall, the linear solver presents reasonable efficiency for SDLS despite the fact that the system is non-SPD.

V. CONCLUDING REMARKS AND FURTHER DISCUSSION

V.A. Conclusions

In this work, we proposed a subdomain discontinuous LS discretization method for solving neutral particle transport. It solves a LS problem in each region of the problem assuming spatially uniform cross sections within each region and couples the contiguous regions with discontinuous interface conditions. We demonstrated that our formulation preserves conservation in each subdomain and gives smaller numerical error than either SAAF or standard LS methods.

Though SDLS is angularly discretized with the S_N method in this work, P_N would be applicable in the angular discretization as well. Therein, LS P_N (Refs. 32, 33, and 34) is applied in each subdomain with a Mark-type boundary

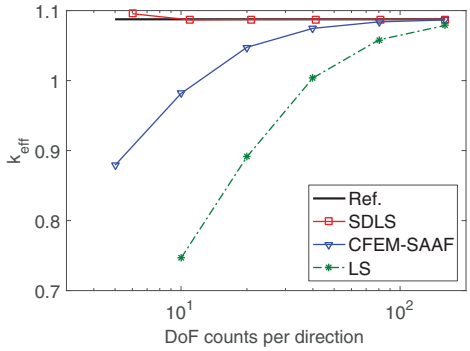

(a) k_{eff} values from different methods.

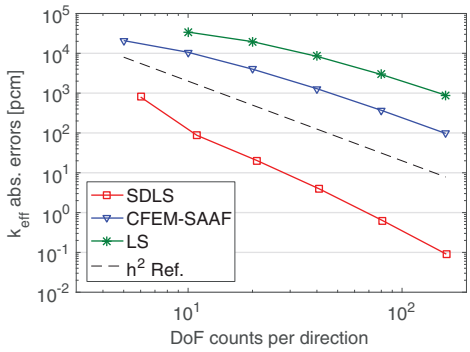

(b) Absolute errors in pcm.

Fig. 5. The k-eigenvalue results.

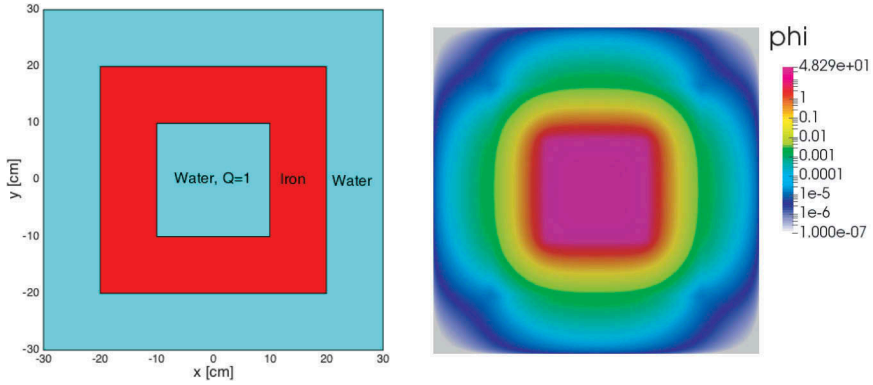

(a) Problem configuration. (b) Scalar flux distribution from reference.

Fig. 6. Results from the iron-water problem.

TABLE IV

Material Cross Sections in One-Group Iron-Water Test

Materials	σ_t (cm^{-1})	σ_s (cm^{-1})
Water	3.2759	3.2656
Iron	1.1228	0.9328

condition used as the interface condition.[35] Further, since SDLS allows the discontinuity on the subdomain interface, different angular schemes, e.g., S_N and P_N, can be used in different subdomains. In fact, the angular coupling is desirable for SAAF in the Rattlesnake code suite[36] at Idaho National Laboratory. An initial implementation of the coupling has been developed in Ref. 37 through enforcing strong continuity of the angular flux on the coupling subdomain interfaces. And, later, the interface discontinuity is applied to SAAF to allow an effectively improved coupling scheme reported in Refs. 30 and 38 and implemented in Rattlesnake to improve the neutronics calculations.

V.B. Future Recommendations

We restrict the method to the configuration in which the total cross section is uniform within subdomains. For cases in which total cross sections vary smoothly within subdomains, one could simply weight the subdomain functional with the reciprocal total cross section while weighting the subdomain interface functional with 1. The rationale is such that the weak form resembles the conservative CFEM-SAAF in the corresponding subdomain with spatially varying cross sections (see Ref. 6 for demonstration).

Another interesting direction is to explore the effects of reentrant curved subdomain interfaces, which the current study does not consider. The efficacy of the method and accordingly the solving techniques in these cases are not known and are worthy of investigation.

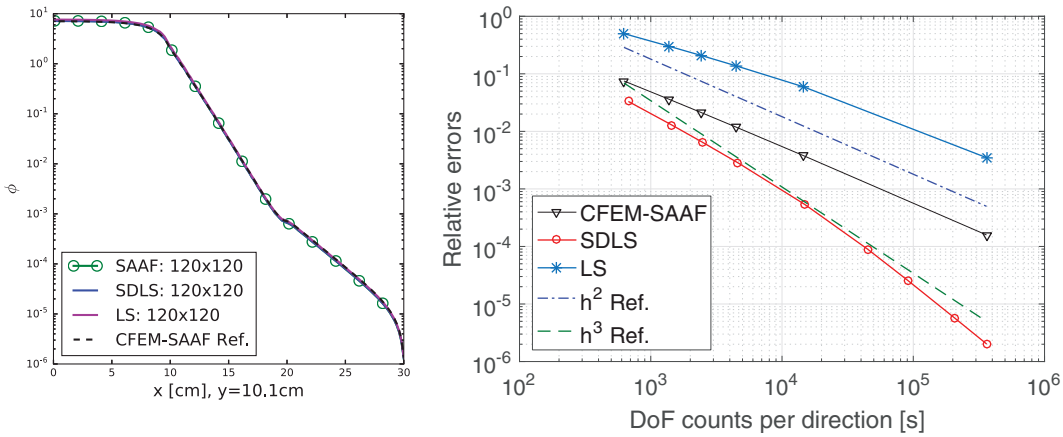

(a) Line-out plot for $x = 10.1$ cm. (b) Relative iron absorption errors.

Fig. 7. Results from the iron-water problem.

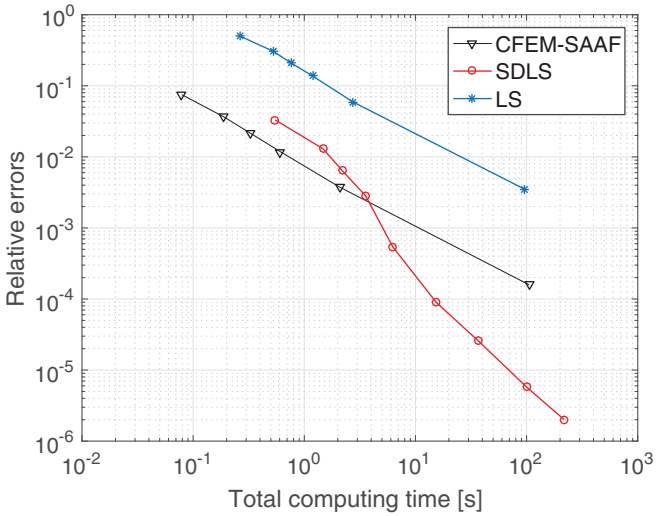

Fig. 8. Relative errors of absorption rate in iron versus total computing time.

Acknowledgments

W. Zheng is thankful to B. Turksin from Oak Ridge National Laboratory for the suggestions on multi-D implementation, Y. Wang from Idaho National Laboratory for his suggestions to make the notation simple and clear, and H. Hammer from Texas A&M Nuclear Engineering for running reference tests. Finally, we wish to thank the anonymous reviewers for their invaluable advice on improving the paper to its current shape.

This project was funded by the U.S. Department of Energy Nuclear Energy University Program research grant from Battelle Energy Alliance, LLC–Idaho National Laboratory, contract C12-00281.

ORCID

Weixiong Zheng http://orcid.org/0000-0003-1372-4123

References

1. M. L. ADAMS, "Discontinuous Finite Element Transport Solutions in Thick Diffusive Problems," *Nucl. Sci. Eng.*, **137**, *3*, 298 (2001); https://doi.org/10.13182/NSE00-41.
2. J. E. MOREL and J. M. McGHEE, "A Self-Adjoint Angular Flux Equation," *Nucl. Sci. Eng.*, **132**, *3*, 312 (1999); https://doi.org/10.13182/NSE132-312.
3. C. J. GESH, "Finite Element Methods for Second Order Forms of the Transport Equation," PhD Dissertation, Texas A&M University (1999).
4. C. J. GESH and M. L. ADAMS, "Finite Element Solutions of Second-Order Forms of the Transport Equation at the Interface Between Diffusive and Non-Diffusive Regions," *Proc. Int. Topl Mtg. Mathematical Methods for Nuclear Applications* (*M&C 2001)*, Salt Lake City, Utah, September 2001, American Nuclear Society (2001).
5. Y. ZHANG, "Even-Parity S_N Adjoint Method Including SP_N Model Error and Iterative Efficiency," PhD Dissertation, Texas A&M University (2014).
6. W. ZHENG, "Least-Squares and Other Residual Based Techniques for Radiation Transport Calculations," PhD Dissertation, Texas A&M University (2016).
7. J. HANSEN et al., "A Least-Squares Transport Equation Compatible with Voids," *J. Comput. Theor. Transport*, **43**, *1–7*, 374 (2015); https://doi.org/10.1080/00411450.2014.927364.
8. B. A. FINLAYSON and L. E. SCRIVEN, "The Method of Weighted Residuals—A Review," *Appl. Math. Rev.*, **19**, *9*, 735 (1966); https://www.researchgate.net/publication/284091948_The_method_of_weighted_residuals_-_A_review (current as of Dec. 6, 2016).
9. E. D. EASON, "A Review of Least-Squares Methods for Solving Partial Differential Equations," *Int. J. Numer. Meth. Eng.*, **10**, 1021 (1976); https://doi.org/10.1002/(ISSN)1097-0207.
10. J. LIABLE and G. PINDER, "Least-Squares Collocation Solution of Differential Equations on Irregularly Shaped Domains Using Orthogonal Meshes," *Numer. Meth. Partial Differ. Equ.*, **5**, 347 (1989); https://doi.org/10.1002/num.1690050406.
11. R. B. LOWRIE and P. L. ROE, "On the Numerical Solution of Conservation Laws by Minimizing Residuals," *J. Comput. Phys.*, **113**, *2*, 304 (1994); https://doi.org/10.1006/jcph.1994.1137.
12. J. L. GUERMOND, "A Finite Element Technique for Solving First Order PDEs in L^p," *SIAM J. Numer. Anal.*, **42**, *2*, 714 (2004); https://doi.org/10.1137/S0036142902417054.
13. P. BOCHEV and M. GUNZBURGER, "Least-Squares Finite Element Methods," *Proc. Int. Congress of Mathematicians* (*ICM 2006)*, Madrid, Spain, August 22–30, 2006, European Mathematical Society (2006).
14. W. ZHENG and R. G. McCLARREN, "Non-Oscillatory Reweighted Least Square Finite Element Method for S_N Transport," *Trans. Am. Nucl. Soc.*, **113**, 688 (2015).
15. W. ZHENG and R. G. McCLARREN, "Non-Oscillatory Reweighted Least Square Finite Element for Solving P_N Transport," *Trans. Am. Nucl. Soc.*, **113**, 692 (2015).
16. W. ZHENG and R. G. McCLARREN, "Effective Non-Oscillatory Regularized L_1 Finite Elements for Particle Transport Simulations," ArXiv e-prints arXiv:1612.05581.
17. C. DRUMM, "Spherical Harmonics (P_n) Methods in the Sceptre Radiation Transport Code," *Proc. Joint Int. Conf. Mathematics & Computation* (*M&C+SNA+MC 2015)*,

Nashville, Tennessee, April 19–23, 2015, American Nuclear Society (2015).

18. V. M. LABOURE, R. G. McCLARREN, and Y. WANG, "Globally Conservative, Hybrid Self-Adjoint Angular Flux and Least-Squares Method Compatible with Void," ArXiv e-prints arXiv:1605.05388.
19. J. R. PETERSON et al., "Conservative Nonlinear Diffusion Acceleration Applied to the Unweighted Least-Squares Transport Equation in MOOSE," *Proc. Joint Int. Conf. Mathematics & Computation (M&C+SNA+MC 2015)*, Nashville, Tennessee, April 19–23, 2015, American Nuclear Society (2015).
20. D. A. KNOLL, H. PARK, and K. SMITH, "Application of the Jacobian-Free Newton-Krylov Method to Nonlinear Acceleration of Transport Source Iteration in Slab Geometry," *Nucl. Sci. Eng.*, **167**, *2*, 122 (2011); https://doi.org/10.13182/NSE09-75.
21. Y. WANG, H. ZHANG, and R. C. MARTINEAU, "Diffusion Acceleration Schemes for Self-Adjoint Angular Flux Formulation with a Void Treatment," *Nucl. Sci. Eng.*, **176**, *2*, 201 (2014); https://doi.org/10.13182/NSE12-83.
22. G. I. BELL and S. GLASSTONE, *Nuclear Reactor Theory*, 3rd ed., Krieger Publishing Company, Princeton, New Jersey (1985).
23. R. LIN, "Discontinuous Discretization for Least-Squares Formulation of Singularity Perturbed Reaction-Diffusion Problems in One and Two Dimensions," *SIAM J. Numer. Anal.*, **47**, *1*, 89 (2008); https://doi.org/10.1137/070700267.
24. V. M. LABOURE, Y. WANG, and M. D. DeHART, "Least-Squares P_N Formulation of the Transport Equation Using Self-Adjoint Angular Flux Consistent Boundary Conditions," *Proc. PHYSOR 2016*, Sun Valley, Idaho, May 1–5, 2016, American Nuclear Society (2016).
25. W. BANGERTH et al., "The deal.ii Library, Version 8.2," in "Archive of Numerical Software," Vol. 3, No. 100 (2015).
26. H. A. VAN DER VORST, "Bi-CGSTAB: A Fast and Smoothly Converging Variant of Bi-CG for the Solution of Nonsymmetric Linear Systems," *SIAM J. Sci. Stat. Comput.*, **13**, *2*, 631 (1992); https://doi.org/10.1137/0913035.
27. D. R. KINCAID and E. W. CHENEY, *Numerical Analysis: Mathematics of Scientific Computing*, 3rd ed., Cengage Learning Inc., Belmont, California (2001).
28. J. J. JARRELL, "An Adaptive Angular Discretization Method for Neutral-Particle Transport in Three-Dimensional Geometries," PhD Dissertation, Texas A&M University (2010).
29. W. REED, "New Difference Schemes for the Neutron Transport Equation," *Nucl. Sci. Eng.*, **46**, *2*, 309 (1971); https://doi.org/10.13182/NSE46-309.
30. W. ZHENG, Y. WANG, and M. DeHART, "Multiscale Capability in Rattlesnake Using Contiguous Discontinuous Discretization of Self-Adjoint Angular Flux Equation," INL/EXT-16-39793, Idaho National Laboratory (2016).
31. C. L. CASTRIANNI and M. L. ADAMS, "A Nonlinear Corner-Balance Spatial Discretization for Transport on Arbitrary Grids," *Nucl. Sci. Eng.*, **128**, *3*, 278 (1998); https://doi.org/10.13182/NSE98-A1956.
32. W. ZHENG and R. G. McCLARREN, "Accurate Least-Squares P_N Scaling Based on Problem Optical Thickness for Solving Neutron Transport Problems," *Prog. Nucl. Energy*," **101**, part C, 394 (Nov. 2017); https://doi.org/10.1016/j.pnucene.2017.06.001.
33. T. A. MANTEUFFEL and K. J. RESSEL, "Least-Squares Finite-Element Solution of the Nuetron Transport Equation in Diffusive Regimes," *SIAM J. Numer. Anal.*, **35**, *2*, 806 (1998); https://doi.org/10.1137/S0036142996299708.
34. E. VARIN and G. SAMBA, "Spherical Harmonics Finite Element Transport Equation Solution Using a Least-Square Approach," *Nucl. Sci. Eng.*, **151**, *2*, 167 (2005); https://doi.org/10.13182/NSE05-A2538.
35. R. SANCHEZ and N. J. McCORMICK, "A Review of Neutron Transport Approximations," *Nucl. Sci. Eng.*, **80**, *4*, 481 (1982); https://doi.org/10.13182/NSE80-04-481.
36. Y. WANG, "The Method of Manufactured Solutions for RattleSnake, A SN Radiation Transport Solver Inside the MOOSE Framework," INL/CON–12-24712, Idaho National Laboratory (2012).
37. S. SCHUNERT et al., "Hybrid P_N-S_N Calculations with SAAF for the Multiscale Transport Capability in Rattlesnake," *Proc. PHYSOR 2016*, Sun Valley, Idaho, May 1–5, 2016, American Nuclear Society (2016).
38. Y. WANG et al., "Hybrid P_N-S_N with Lagrange Multiplier and Upwinding for the Multiscale Transport Capability in Rattlesnake," *Prog. Nucl. Energy*, **101**, part C, 381 (2017); https://doi.org/10.1016/j.pnucene.2017.03.020.